Defence Science Journal, Vol. 71, No. 4, July 2021, pp. 535-544, DOI : 10.14429/dsj.71.15798

Nonlinear Extended State Observer-based Active Disturbance Rejection Control of a Laser Seeker System

Abdellah Ferdjali[#], Taki-Eddine Lechekhab[#], Stojadin Manojlović[#], Momir Stanković[#,*], Rafal Madonski[@], and Dimitrije Bujakovic[#]

[#]*Military academy, University of Defence, Belgrade, Serbia*
[@]*International Energy College, Jinan University, Guangzhou, China*
[*]*E-mail: momir_stankovic@yahoo.com*

ABSTRACT

In this paper, the laser seeker control problem is solved in the framework of active disturbance rejection control (ADRC). The considered problem, which consists of laser seeker stabilisation and target tracking, is expressed here as a regulation problem. A nonlinear extended state observer (NESO) with varying gains is used to improve the performance of linear ESO (LESO), and thus enable better control performance in both transient period and steady-state, with lower control effort. Based on a detailed analysis of system disturbances, a special ADRC tuning method is proposed. The stability of the overall control structure is analysed with a description function method. Through comparative simulations LESO-based and the introduced NESO-based ADRC for the laser seeker system, the advantages of the proposed scheme are shown.

Keywords: Active Disturbance Rejection Control (ADRC); Nonlinear Extended State Observer (NESO); Laser seeker control

1. INTRODUCTION

High precision of laser guided weapons mainly depends on tracking performance and robustness of laser seekers. Related to other types, such as radio frequency (RF) seekers, laser seekers are featured with high guidance accuracy, strong anti-jamming ability, simple structure and low cost[1]. In laser homing guided weapons, laser seekers are usually referred to as semi-active systems, because the transmitter (laser target designator) is not co-located with the seeker[2,3]. The main functions to be carried out by laser seeker in guidance loop are detection, acquisition and tracking of designated target, signal processing and computation of error signals, necessary for guidance computer.

Basic components of laser seeker include a stabilisation platform and a photo-electric device mounted on the platform. The incoming laser energy, reflected from the target, is detected by a photosensitive element in the photo-electric device and transformed into electrical displacement signals. The displacement signals contain information about the target line of sight (LOS) angular positions in the seeker field of view (FOV)[2,4]. Based on these signals, the stabilisation platform directs the seeker (with two servo systems) to align its optical axis and target LOS. The platform control software has to isolate the optical axis from various external and internal disturbances, while continuously enabling precise target pointing and validating data for the guidance computer. Consequently, the core purpose of the laser seeker control system is to stabilize the optical axis and to track the LOS kinematics in the seeker FOV[5]. This goal, however, is challenging due to several aspects, described next.

In the laser seeker systems, a quadrant photo detector (QPD) is one of the most applied photosensitive position sensor, due to its small dimensions, simple processing electronics, and low cost. The reflected laser energy through focus optics is transformed to a spot on the QPD surface. The sensitive surface of the QPD is divided into four quadrants in order to convert laser spot energy to two displacement signals, thus enabling LOS angular orientation in both (horizontal and vertical) planes. Including both optical and electrical nonlinear phenomena, the QPD has considered as nonlinear component, regardless of the utilised QPD signals processing algorithm[6].

For variety of the guidance methods, the most important information is the LOS rate. In contrast to strapdown seekers, in gimbaled seekers the photo-electronic device is mounted on a two-axis gimbal construction, which enables the photo-electronic device to move independently to missile body and to directly measure LOS angle and LOS angle rate in the inertial coordinate frame. Modelling of the gimbal platform is unfortunately task. Although the mathematical models, given in forms of kinematic and dynamic equations, are well known and include phenomena such as cross-couplings, mass unbalance, nonlinearities, etc., there is a significant number of parameters to be determined. The additional challenge is the influence of different unpredictable and unmeasurable external and internal disturbances.

Received : 04 May 2020, Revised : 23 February 2021
Accepted : 26 February 2021, Online published : 01 July 2021

There are various control strategies for solving the laser seeker control problem, including both classical and modern control techniques. The proportional-integral-derivative (PID) controllers are still used, but rather in their improved versions like in[7], where cascaded structure is employed in the stabilising loop, or in[8] with fuzzy-PID controller and self-adapting parameters. Formulation of the seeker stabilisation as a robust H_∞ optimisation problem is shown in[9], with a feedback-stabilisation controller and a feed forward-tracking controller. Based on a minimisation of an appropriately defined cost function, optimal LQG/LTR controllers are introduced in[10], with disturbances and sensor noises modelled as stochastic inputs. In order to cope with the seeker nonlinear dynamics, papers[11,12] implement sliding-mode control (and its modifications to avoid the chattering problem). However, the common drawback of the above approaches is the dependency of control performance on precise system modelling.

In the last few years, there has been an intensive effort to formulate and solve the seeker control problem in the framework of active disturbance rejection control (ADRC)[13-15]. The ADRC represents a general robust approach that can be tailored to many control problems[16-19]. In this concept, external disturbances, unmodelled system dynamics, and parameter uncertainties are treated as a single (total) disturbance, which should be rejected in each time instant. Such lumped disturbance signal can be reconstructed in real-time using an observer, namely an extended state observer (ESO), and rejected simultaneously by an appropriate control law. Consequently, the uncertain linear/nonlinear system can be transformed into an integral-chain form of *n*-th order, where *n* is the system relative degree, and such structure can effectively be controlled with a simple state feedback control algorithm. It should be noted that the ADRC approach was originally developed as a nonlinear structure that uses nonlinear functions in the ESO and the control law[20]. Although the nonlinear ADRC is potentially more effective and generally provides better system performance, its linearised and parameterised form[21] is considered to be more practical solution due to simpler design and smaller number of adjustable parameters. The detailed theoretical studies of the nonlinear ADRC, including convergence and stability analysis, are presented in[22-25].

According to author's best knowledge, there has been limited research that deals with the use of nonlinear ADRC in laser seeker systems, which constitutes the motivation of this work. The main idea of this paper is thus the introduction of the ADRC structure, based on NESO and a linear control law, capable of effectively compensating different types of disturbances in azimuth/elevation channel of the laser seeker system of guided missile. In the work, the laser seeker control problem that consists of laser seeker stabilisation and manoeuvring target tracking problem, is expressed as a regulation problem. Furthermore, a parameter tuning method for the designed controller is proposed, based on the analysis of total disturbance signal in control channels. The stability analysis of the proposed nonlinear control scheme is carried out using limit cycle approach based on a description function method[23,26]. The advantages of the introduced scheme are shown through a quantitative comparison with a linear ADRC solution (as seen in[15]). The comparison analysis is realised through different simulation scenarios focused on angular tracking errors compensations in transient period and steady-state, as well as energy consumption.

2. OVERVIEW OF NONLINEAR ADRC CONCEPT

Let us consider a general *n*th-order nonlinear uncertain system, represented in state-space form[20]:

$$\begin{aligned}
\dot{x}_1(t) &= x_2(t), \\
\dot{x}_2(t) &= x_3(t), \\
&\vdots \\
\dot{x}_n(t) &= \xi(\mathrm{x},t) + bu(t) + d(t), \\
y(t) &= x_1(t),
\end{aligned} \tag{1}$$

where $u(t)$ is the system input, $y(t)$ is the system output, $\mathrm{x} = \left[x_1(t), x_2(t) \ldots x_n(t)\right]^T$ is the state vector, $d(t)$ is the unknown external disturbance, and $\xi(\mathrm{x},t)$ includes the uncertain nonlinear/linear internal dynamics and b represents the system gain, with assumptions that its sign and rough approximation $b_0 \neq 0$ are known.

In order to apply the ADRC approach[20], Eqn (1) is rewritten as:

$$\begin{aligned}
\dot{x}_1(t) &= x_2(t), \\
\dot{x}_2(t) &= x_3(t), \\
&\vdots \\
\dot{x}_n(t) &= f(\mathrm{x},u,t) + b_0 u(t), \\
\dot{x}_{n+1}(t) &= \dot{f}(\mathrm{x},u,t), \\
y(t) &= x_1(t).
\end{aligned} \tag{2}$$

where

$$f(\mathrm{x},u,t) = \xi(\mathrm{x},t) + d(t) + (b - b_0)u(t), \tag{3}$$

is the total disturbance. The idea to treat the uncertain dynamics and the external disturbances as a single always-observable disturbance term $f(\mathrm{x},u,t)$, which is represented as an extended state $x_{n+1}(t)$, is the essence of ADRC approach and it is discussed in detail in[27].

To design ADRC controller, the real-time estimation of the system Eqn (2) states are needed. Therefore, a NESO is proposed:

$$\begin{aligned}
\dot{\hat{x}}_1(t) &= \hat{x}_2(t) + \beta_1 \phi_1(\varepsilon_1(t)), \\
\dot{\hat{x}}_2(t) &= \hat{x}_3(t) + \beta_2 \phi_2(\varepsilon_1(t)), \\
&\vdots \\
\dot{\hat{x}}_n(t) &= \hat{x}_{n+1}(t) + b_0 u(t) + \beta_n \phi_n(\varepsilon_1(t)), \\
\dot{\hat{x}}_{n+1}(t) &= \beta_{n+1} \phi_{n+1}(\varepsilon_1(t)),
\end{aligned} \tag{4}$$

where $\hat{\mathrm{x}} = \left[\hat{x}_1(t), \hat{x}_2(t) \ldots \hat{x}_n(t), \hat{x}_{n+1}(t)\right]^T$ is the estimation state vector, $\beta_1, \beta_2, \ldots \beta_n, \beta_{n+1}$ are the observer gains, $\varepsilon_1(t) = x_1(t) - \hat{x}_1(t)$ is the estimation error, and $\phi_i(\varepsilon_1(t))$, $i = 1, 2, \ldots n, n+1$, are nonlinear functions, defined as[20]:

$$\phi_i(\varepsilon_1(t)) = fal(\varepsilon_1(t),\alpha_i,\delta\ ) = \begin{cases} \varepsilon_1(t)/\delta^{1-\alpha_i}\ , & |\varepsilon_1(t)| \le \delta \\ |\varepsilon_1(t)|^{\alpha_i}\ sign(\varepsilon_1(t)), & |\varepsilon_1(t)| > \delta \end{cases} \tag{5}$$

where δ and α_i are predetermined coefficients that define linear range of function and function power. One can note that choosing $\alpha_i < 1$ main characteristic of Eqn (5) can be colloquially described as "small error-big gain; big error-small gain". In this way, the impact of the observer gains is reduced in the transient period (when the estimation error is big) and it enables quick recovery of the system states. On the other hand, the big function gain, when the error is small, provides high performance in the steady-state. However, it should be noted that in order to reduce the effect of the measurement noise, the system steady-state error $\varepsilon_1(\infty)$ should be located in the nonlinear range, i.e. $\delta < \varepsilon_1(\infty)$. Also, one can see that the Eqn (5) can be turned into a linear one by choosing $\alpha_i = 1$.

To reject the total disturbance $f(\mathrm{x},u,t)$, control signal is designed based on the estimation $\hat{x}_{n+1}(t)$ as:

$$u(t) = \frac{u_0(t) - \hat{x}_{n+1}(t)}{b_0}. \tag{6}$$

The control law $u_0(t)$ generally has nonlinear form:

$$u_0(t) = r^{(n)}(t) + \sum_{i=1}^{n} k_i \phi_i(e_i(t),\alpha_i^{'},\delta^{'}) \tag{7}$$

where k_i are the controller gains and nonlinear functions $\phi_i(\cdot)$ has same structure as in Eqn (5), but in this case is designed for feedback error $e_i(t) = r^{(i-1)}(t) - \hat{x}_i(t)$, where $r^{(i)}(t)$ is ith derivative of the reference signal $r(t)$. In this paper, by choosing $\alpha_i^{'} = 1$, the linear form of Eqn (7) is adopted, and it is described in the following.

3. NESO-BASED ADRC OF LASER SEEKER SYSTEM

3.1 Dynamical model of the laser seeker

The functional scheme of the laser seeker, with QPD as sensing element, is presented in Fig. 1. Independent orientation of the seeker in both planes is enabled by two gimbals, inner (pitch) and outer (yaw) gimbal. Owing to good stabilising performances, the massive precession gyro (PG) is mounted on the inner gimbal, which allows it to spin freely around its principal axis x_D with angular velocity $\vec{\Omega}$. Azimuth gimbal, together with PG, can rotate in vertical plane around z_D axis, and complete construction, coupled with yaw gimbal, can rotate in horizontal plane around y_D axis. Optical system with QPD, mounted in front of PG so the seeker optical axis passes through its centre, tracks the angular orientation of the gyro in both, horizontal and vertical planes.

The optical system detects the misalignment of the LOS and optical axis, i.e. angular errors δ_v and δ_h, and generates two displacement signals ε_v and ε_h, respectively. The amplified displacement signals ε_{vA} and ε_{hA}, as error signals in the vertical and horizontal planes, are sent to the controllers C1 and C2 for control signals calculation, and to guidance computer (GC) for guidance law forming. Controllers outputs u_y and u_x, generated by torque motors TM2 and TM1, are

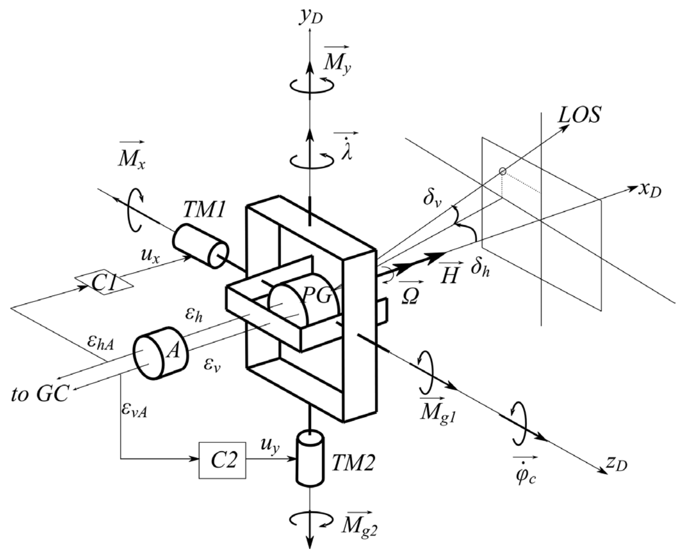

Figure 1. The functional scheme of the laser seeker.

transformed into correction moments $\vec{M}_x$ and $\vec{M}_y$, which cause gyro precession movement, forcing the gimbals to rotate in order to eliminate angular errors δ_v and δ_h.

The correction moments $\vec{M}_x$ and $\vec{M}_y$ are simultaneously compensated with gyro moments $\vec{M}_{g1} = \vec{H} \times \dot{\vec{\lambda}}_c$ and $\vec{M}_{g2} = \vec{H} \times \dot{\vec{\varphi}}_c$, respectively, where $\vec{H}$ is the angular momentum vector of the gyro. In equilibrium holds:

$$\begin{aligned} \vec{M}_x &= -\vec{M}_{g1} = \dot{\vec{\lambda}}_C \times \vec{H} \\ \vec{M}_y &= -\vec{M}_{g2} = \dot{\vec{\phi}}_C \times \vec{H} \end{aligned}, \tag{8}$$

and, since the vectors $\dot{\vec{\lambda}}_c$ and $\dot{\vec{\varphi}}_c$, as well as the angular momentum vector $\vec{H}$ are approximately orthogonal, Eqn (8) can be rewritten as:

$$\begin{aligned} \dot{\lambda}_C &= M_x / H \\ \dot{\varphi}_C &= M_y / H \end{aligned}. \tag{9}$$

Previous equation shows that in the disturbance free case, precession angular rates of the gyro $\dot{\lambda}_c$ and $\dot{\varphi}_c$ are directly proportional to the correction moments M_x and M_y, respectively. By utilising M_x and M_y the angular errors δ_v and δ_h are reduced, respectively.

According to the functional scheme in Fig. 1, the schematic diagram of the laser seeker is formed and it can be seen in Fig. 2. The LOS dynamics is primarily influenced by target manoeuvre and missile vibrations. In this case, the external disturbances caused by missile vibrations are modelled with disturbing moments M_{px} and M_{py}, as additional moments to the correcting moments. Furthermore, λ and φ denote the azimuth and elevation angle of the LOS, respectively. The QPD has nonlinear characteristics[6], but if the laser spot is near the centre of the QPD, the characteristics can be approximated as linear, with the same coefficient K_{QPD} in both planes. Also, supposing that the torque motors are of the same construction, they can be described with parameter K_{TM}. Similarly, the amplifiers can be modelled with the same coefficient K_A.

It should be noted that if the target is in the QPD field of view the displacement signals ε_{vA} and ε_{hA} are generated and their dynamics depend on LOS dynamics (manoeuvring target tracking problem) and platform vibrations (stabilisation problem). Since these signals represent error signals, from the control point of view, this problem can be treated as a regulation problem with reference inputs in both channels settled as $r_x = r_y = 0$ (see Fig. 2).

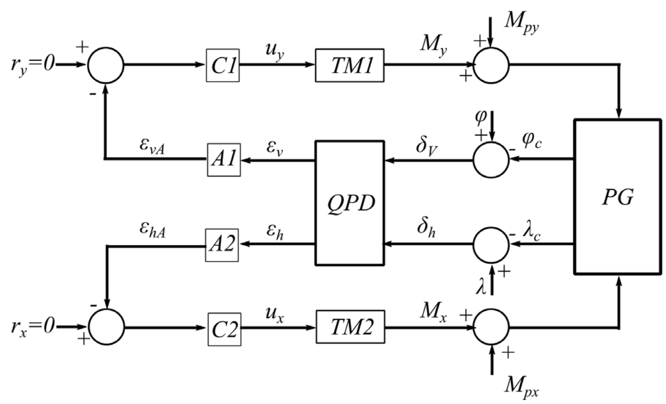

Figure 2. The schematic diagram of the laser seeker.

3.2 NESO-based Controller Design

As previously described, the QPD, torque motors and amplifiers can be modelled as linear components: $(\varepsilon_y, \varepsilon_x) = K_{QPD}(\delta_y, \delta_x)$, $(M_y, M_x) = K_{TM}(u_y, u_x)$ and $(\varepsilon_{yA}, \varepsilon_{xA}) = K_A(\varepsilon_y, \varepsilon_x)$, respectively. In the presence of external disturbances, including the target manoeuver, and modelling the QPD, torque motors and amplifiers as linear components, the dynamics of the amplified displacement signals can be described with[15]:

$$\begin{aligned} \dot{\varepsilon}_{xA}(t) &= -\frac{K_A K_{QPD} K_{TM}}{H} u_x(t) - \frac{K_A K_{QPD}}{H} M_{px}(t) + K_A K_{QPD} \dot{\lambda}(t) \\ \dot{\varepsilon}_{yA}(t) &= -\frac{K_A K_{QPD} K_{TM}}{H} u_y(t) - \frac{K_A K_{QPD}}{H} M_{py}(t) + K_A K_{QPD} \dot{\varphi}(t) \end{aligned} \tag{10}$$

If one reformulates Eqn (10) into ADRC form Eqn (2), gives:

$$\begin{aligned} \dot{\varepsilon}_{xA}(t) &= b_{0x} u_x(t) + f_x(t) \\ \dot{\varepsilon}_{yA}(t) &= b_{0y} u_y(t) + f_y(t) \end{aligned}, \tag{11}$$

where $b_{0x} = b_{0y}$ are the best approximations of the input gains $b_x = b_y = -\frac{K_A K_{QPD} K_{TM}}{H}$, and

$$\begin{aligned} f_x(t) &= -\frac{K_A K_{QPD}}{H} M_{px}(t) + K_A K_{QPD} \dot{\lambda}(t) + \Delta b_{0x} u_x(t) \\ f_y(t) &= -\frac{K_A K_{QPD}}{H} M_{py}(t) + K_A K_{QPD} \dot{\varphi}(t) + \Delta b_{0y} u_y(t) \end{aligned} \tag{12}$$

are the total disturbances in the azimuth and elevation channels, respectively. It should be noted that the QPD nonlinearity, the torque motors and amplifiers parameters uncertainty are included into Δb_{0x} and Δb_{0y}, i.e. $\Delta b_{0x} = b_x - b_{0x}$ and $\Delta b_{0y} = b_y - b_{0y}$. From Eqn (11) it is evident that the dynamics of the both channels are similar and of the first order. Therefore, in the following the design of the NADRC for the elevation channel (in the vertical plane) will be described, and the similar procedure can be performed for the azimuth channel.

Choosing the state vector as $\mathrm{x}(t) = \left[x_1(t) \quad x_2(t)\right]^T = \left[\varepsilon_{yA}(t) \quad f_y(t)\right]^T$ and *fal* function parameters as $\alpha_1 = 1, \alpha_2 = 0.5$ and $\delta = 0.05$, the NESO Eqn (4) have form:

$$\begin{aligned} \dot{\hat{x}}_1(t) &= \hat{x}_2(t) + b_{0y} u_y(t) + \beta_1 \varepsilon_1(t) \\ \dot{\hat{x}}_2(t) &= \beta_2 \phi_2(\varepsilon_1(t)) \end{aligned} \tag{13}$$

Additionally, according to comparison of nonlinear observer Eqn (13) and its linear equivalent extended state observer (LESO), based on numerical optimisation methods, the observer parameters should be set, as suggested in[28]:

$$\beta_1 = 2\omega_0, \beta_2 = \omega_0^2 / 3 \ , \tag{14}$$

where ω_0 is the linear observer bandwidth. The total disturbance is rejected according to Eqn (6) with linear form of the control rule Eqn (7):

$$u_y(t) = \frac{-k_1 \hat{x}_1(t) - \hat{x}_2}{b_{0y}}, \tag{15}$$

The controller parameter is set as $k_1 = \omega_c$, where ω_c represents the desired closed-loop system bandwidth[21].

3.3 Parameters tuning

From the previous analysis, it is obvious that design of NESO-based controller requires the appropriate tuning of parameters ω_c and ω_0. According to[28], the steady-state estimation errors of the NESO Eqn (13) can be obtained as:

$$\begin{aligned} \left|\varepsilon_1(t)\right| &= \left|\hat{x}_1(t) - x_1(t)\right| \le \left(\frac{h(t)}{\beta_2}\right)^2; \\ \left|\varepsilon_2(t)\right| &= \left|\hat{x}_2(t) - x_2(t)\right| \le \beta_1 \left(\frac{h(t)}{\beta_2}\right)^2, \end{aligned} \tag{16}$$

where $h(t) = \dot{f}_y(t)$. Further, assuming that $h(t)$ is a constant function ($h(t) = h_0$) and $\delta < \left|\varepsilon_1(t)\right|$, for the NESO gains tuned as Eqn (14), the steady-state errors Eqn (16) are constants and have forms:

$$\left|\varepsilon_1\right| = \left(\frac{3h_0}{\omega_0^2}\right)^2; \quad \left|\varepsilon_2\right| = 2\omega_0 \left(\frac{3h_0}{\omega_0^2}\right)^2 \tag{17}$$

In the same manner, choosing $\alpha_2 = 1$, $\beta_1 = 2\omega_0$ and $\beta_2 = \omega_0^2$ in Eqn (13), the steady-state error of equivalent LESO can be obtained as:

$$\left|\varepsilon_1^{'}\right| = \frac{h_0}{\omega_0^2}; \quad \left|\varepsilon_2^{'}\right| = \frac{2h_0}{\omega_0}. \tag{18}$$

Comparing Eqn (17) and Eqn (18), it can be obtained that NESO has lower steady-state errors than LESO if $h_0 < \omega_0^2 / 9$. Therefore, tuning $\omega_0 > h_{0\max} / 9$, where $h_{0\max}$ is maximal value of total disturbance derivative h_0, it is achieved that NESO has better steady-state performances than appropriate LESO for $h_0 \in (0, h_{0\max})$.

In order to obtain $h_{0\max}$ for considered elevation control channel of the laser seeker system, the structure of the total disturbance Eqn (12) is analysed. It is evident that it depends on external vibration torque disturbance $M_{py}(t)$, LOS angle $\varphi(t)$ and parameter uncertainty Δb_y. However, as the model and parameters of laser system are mostly known, and the influence of $M_{py}(t)$ is significantly lower than the influence of $\varphi(t)$, the Eqn (15) can be approximated as:

$$f_y(t) \approx K_A K_{QPD} \dot{\varphi}(t) \tag{19}$$

and its derivative can be defined as $h(t) \approx K_A K_{QPD} \ddot{\varphi}(t)$. It is evident that $h(t) \approx 0$ in the cases when LOS angle is constant function and ramp function, that correspond to pointing to stationary target and tracking of the target which manoeuvres with constant velocity in sensor FOV, respectively. However, if target manoeuvres with constant acceleration, i.e. when $\varphi(t) = at^2$, the derivative of total disturbance is $h(t) \approx h_0 \approx 2aK_A K_{QPD}$, and its maximal value $h_{0\max}$ depends on parameter *a*. Therefore, the observer bandwidth should be tuned as $\omega_0 > 2a_{\max} K_A K_{QPD} / 9$, where $a_{\max}$ is maximal value of the LOS dynamics parameter *a*.

4. STABILITY ANALYSIS

In this section the stability analysis based on the describing function method[26], is provided. In this manner, the nonlinear function $\phi_2(\varepsilon_1(t))$ is treated as transformation of the error signal, and described with equivalent nonlinear gain ρ:

$$\rho(\varepsilon_1) = \frac{\phi_2(\varepsilon_1(t))}{\varepsilon_1(t)} \tag{20}$$

This nonlinearity is implemented in the NESO Eqn (13) as equivalent gain. Applying Laplace transformation to Eqn (13) and Eqn (15), the NESO-based ADRC system of elevation control channel is converted to frequency domain and described as basic unity feedback form with open loop transfer function:

$$W(\rho, s) = \frac{b_y}{s} \frac{(\beta_2 \rho(\varepsilon_1) + k_1 \beta_1)s + k_1 \beta_2 \rho(\varepsilon_1)}{b_{0y} s(s + \beta_1 k_1)} \tag{21}$$

In order to apply describing function method, Eqn (21) can be reformulated as equivalent form $\rho(\varepsilon_1) G(s)$ with separated nonlinear term $\rho(\varepsilon_1)$ and linear part

$$G(s) = \frac{b_y \beta_2 (s + k_1)}{b_{0y} s^3 + b_{0y} (\beta_1 + k_1) s^2 + b_y k_1 \beta_1 s} \tag{22}$$

The nonlinear part of the system is described using describing function[26]:

$$N(E) = \frac{2}{\pi}\left[\tau - \frac{\delta}{E}\sqrt{1 - \left(\frac{\delta}{E}\right)^2}\right] + \frac{2E^{\alpha_2 - 1}}{\pi} \left[2\left(\frac{\pi}{2} - \tau\right) - \frac{5}{12}\left(\frac{\pi}{2} - \tau\right)^3 + \frac{7}{192}\left(\frac{\pi}{2} - \tau\right)^5\right] \tag{23}$$

where $E > \delta$ represents the amplitude of the error signal $\varepsilon_1(t)$ and $\tau = \arcsin(\delta / E)$. It should be noted that analysis is carried out for $E > \delta$ because in the other case the input remains in linear range.

The characteristic equation of the system in the unity feedback structure can be written as:

$$G(j\omega) = -\frac{1}{N(E)} \tag{24}$$

In Fig. 3 are shown the Nyquist diagrams of the linear part $G(j\omega)$, for $b_{0y} = b_y$ and different $\omega_c \in (1, 10, 100)$ *rad/s* and $\omega_0 = 5\omega_c$, and curve $-1/N(E)$ that represents nonlinear part of the system.

From the Fig. 3 one can see that the parameter tuning does not significantly affect the Nyquist diagrams of $G(j\omega)$ (the plots for different ω_0 are almost overlapped). Further, it can be noticed that the curve $-1/N(E)$ lies on the real axis, and its departure point (for $E = \delta$) is closest point to the Nyquist diagrams of $G(j\omega)$. It is evident that for $\delta = 0.05$, there is no intersection of these curves and it indicates that there is no limit cycle, i.e. the closed-loop system is stable. Further, due to Nyquist diagrams shape (diagrams do not intersect with real axis) it can be concluded that there is no limit cycle for $\delta > 0$ and $0 < \alpha_2 < 1$, and the designed control system is always stable.

It should be noted that the limit cycles in the system can occur when $G(j\omega)$ has higher order than in (22), because in that case Nyquist diagram of $G(j\omega)$ intersects with the real axis and potentially with the curve $-1/N(E)$ [26].

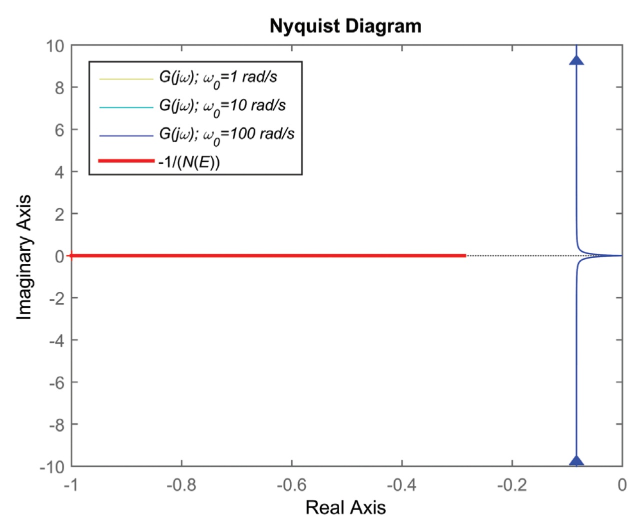

Figure 3. Nyquist diagrams of the linear part $G(j\omega)$ and curve.

5. SIMULATION RESULTS

The comparison study of LESO[15] and NESO-based ADRC laser seeker system is realised through MATLAB/Simulink simulations. It is assumed that both control systems have identical controllers in the vertical and horizontal control channels.

NESO bandwidth ω_0 is set based on the analysis described in Section 3.3. Through numerical simulations of the different engagement scenarios, including appropriate homing guidance methods, based on proportional navigation, and targets with high manoeuvring capabilities (combat aircrafts and missiles), it is obtained that the maximal value of the parameter *a*, in the all cases, is lower than 1. Consequently, for the assumed values of the system parameters K_A=100, $K_{QPD}=1V/rad$, $H=1Nm/rad/s, K_{TM}=0.1Nm/V$, the observer bandwidth should be tuned as $\omega_0 > 2K_A K_{QPD}/9 = 42,4\,rad/s$. On the other hand, the high value of ω_0 leads to increasing observer sensitivity to the measurement noise[29]. Hence, the appropriate ω_0 is tuned as trade-off between those limitations, and in this research is set as $\omega_0 = 50\,rad/s$. Further, based on[21], controller bandwidth is chosen as $\omega_c = \omega_0/(3\div10)$, and it is adopted as $\omega_c = 10\,rad/s$.In the following the comparative analysis of the NESO and linear ESO-based control structures, with previously defined parameters, is carried out for three different scenarios.

Scenario 1:

In this case the target moves in vertical plane, i.e. the LOS angle $\varphi(t)$ vary with constant angular velocity $\dot{\varphi}(t) = 0.5\,rad/s$. The initial position of the laser spot centre is not in the centre of QPD. Actually, the initial angular tracking error in horizontal and vertical channels, $\delta_h(0) = 0.06$ rad and $\delta_v(0) = 0.05$ rad, are assumed. From the control point of view, it corresponds to the system response on ramp and step disturbances in the vertical plane control channel and step disturbance in horizontal plane control channel. The angular errors $\delta_v(t)$ and $\delta_h(t)$, control signals for vertical channel $u_v(t)$, the trajectory of the laser spot centre on QPD surface and the total disturbance estimation error $\varepsilon_2(t)$ in the vertical control and in the horizontal control channel are shown in Fig. 4.

It can be seen that both controllers successfully eliminate disturbances and provide zero steady-state target tracking errors. However, it is obvious that, due to significantly better performance of the total disturbance estimation, response of the system with NESO is faster than with LESO. Also, peak values of the tracking errors in transient period, caused by the constant ESO high gain are effectively reduced by time-varying NESO gains. Regarding control signals, one can see that NESO-based control system provides lower energy consumption and less peak value of the control signal.

Scenario 2:

Rejection of different types of disturbances affecting the laser tracking system are considered in this scenario. The presence of sinusoidal torque disturbances in horizontal plane (platform vibrations of 8.5 Hz and of 0.1 Nm magnitude acts on inputs M_{px}) are supposed. Further, the target manoeuvres, such that both angles $\varphi(t)$ and $\lambda(t)$ change with constant angular accelerations $\ddot{\varphi}(t) = 1\,rad/s^2$ and $\ddot{\lambda}(t) = 2\,rad/s^2$. The initial values are equal to zero, meaning that angular errors are $\delta_h(0) = 0$ and $\delta_v(0) = 0$, in the sensor FOV. Fig. 5 shows angular errors, control signals in horizontal channel control system, spot centre trajectories and the estimation error of the total disturbance in both horizontal and vertical channel for LESO- and NESO-based control systems.

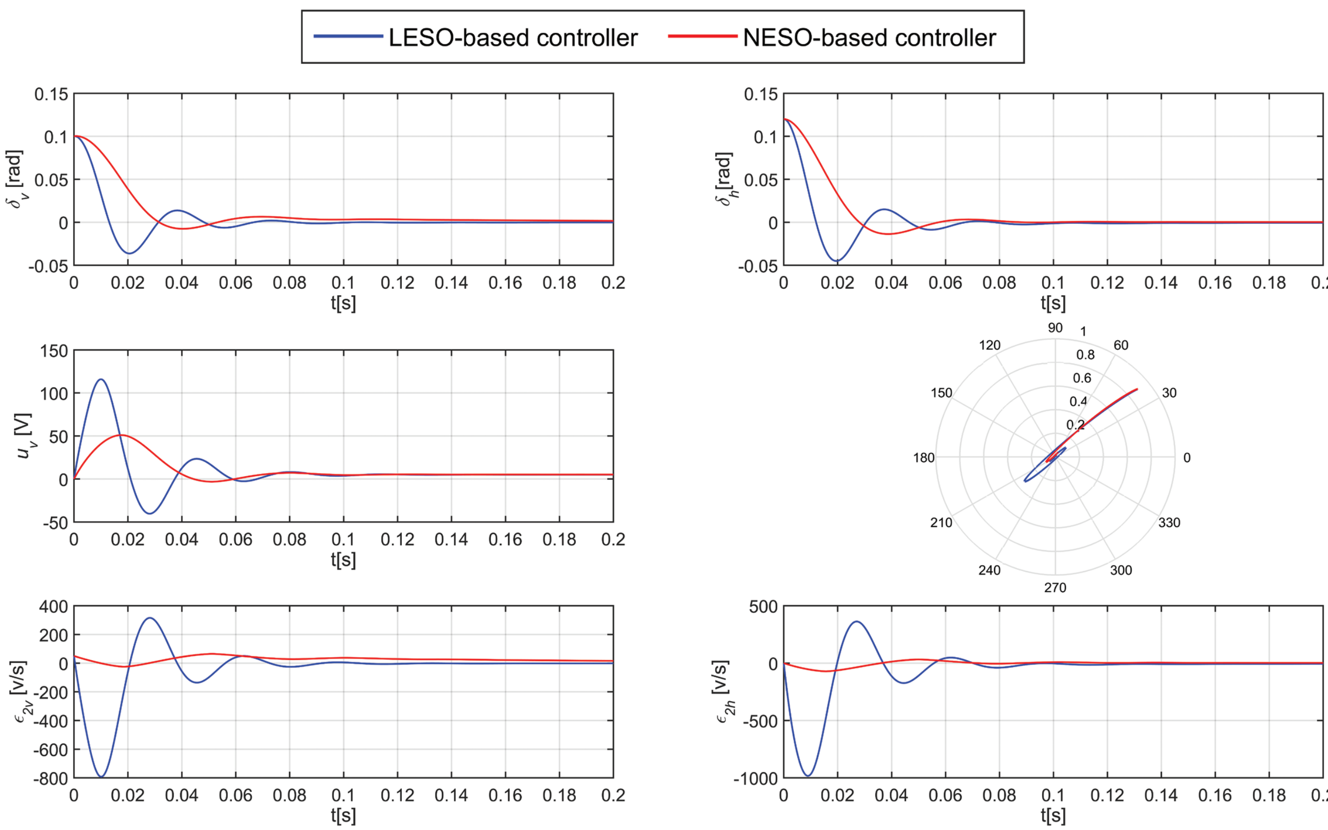

Figure 4. Simulation results for Scenario 1: tracking errors in vertical channel (top left), tracking errors in horizontal channel (top right), control signals in vertical control channel (middle left), spot centre trajectories (middle right), total disturbance error in vertical channel (bottom left), total disturbance error in horizontal channel (bottom right).

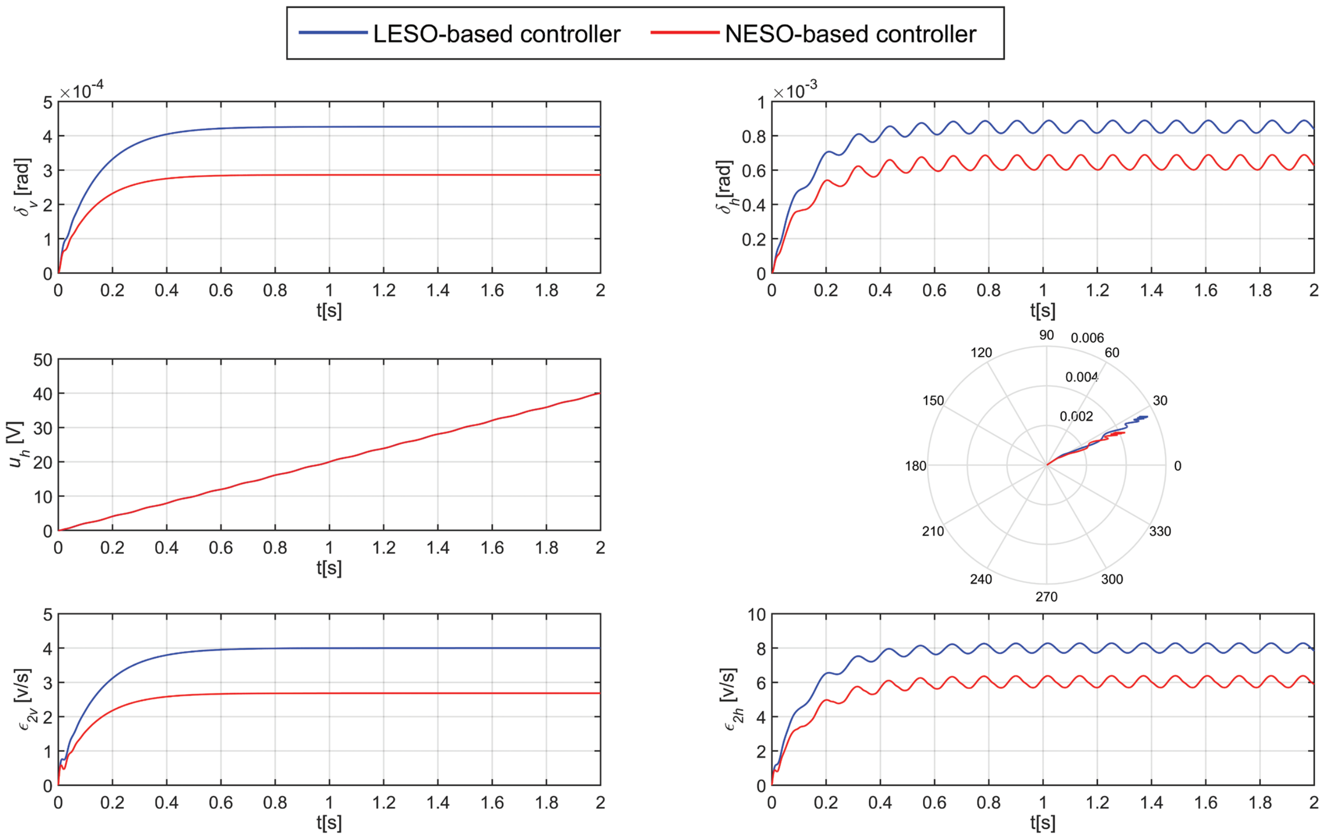

Figure 5. Simulation results for Scenario 2: tracking errors in vertical channel (top left), tracking errors in horizontal channel (top right), control signals in vertical control channel (middle left), spot centre trajectories (middle right), total disturbance error in vertical channel (bottom left), total disturbance error in horizontal channel (bottom right).

It is evident that, due to parabolic varying of LOS angles and sinusoidal torque of external disturbance in the horizontal plane, steady-state error exists in both control channels, but it can be seen that NESO enable lower total disturbance estimation errors compared to the LESO, and consequently it provides better closed-loop steady-state performance of NESO-based control system. The differences in control signals are not visible and that means that both control structures have similar energy consumption. It should be noted that completely rejection of this type of disturbance is possible with generalised ESO structures[15].

Scenario 3:

In this simulation scenario the complex target manoeuvre is supposed, with LOS angles change described as sinusoidal functions:

$$\begin{aligned} \lambda(t) &= 0.15\cos(2t)\, rad \\ \varphi(t) &= 0.15\cos(4t)\, rad. \end{aligned} \tag{25}$$

Initially, the position of laser spot centre is in the centre of sensor FOV, i.e. $\delta_h(0) = \delta_v(0) = 0$. The angular errors, control signals in horizontal channel, spot centre trajectories and the estimation error of the total disturbance in horizontal and vertical channel, for this case, are presented in Fig. 6.

From Fig. 6, one can see that in the steady-state the total disturbance estimation errors and angular errors are oscillating around the zero due to infinite differentiability of the sinusoidal disturbances, but it is obvious that the NESO-based system rejects this type of disturbances better then LESO-based system, with the similar energy consumption.

6. CONCLUSION

In order to improve the laser seeker target tracking accuracy, the active disturbance rejection control, with nonlinear extended state observer (NESO), is presented in this paper. Considering the target manoeuvring and laser platform vibrations, as external disturbances, and QPD nonlinearity and system parameters uncertainty, as internal disturbances, the total disturbances in both, azimuth and elevation channel, are defined. The laser seeker optical axis stabilisation and tracking of manoeuvring target in seeker FOV is formulated as a regulation problem. The efficiency of the proposed control scheme is shown through simulations of representative target tracking scenarios. Stability analysis revealed that closed-loop system with NESO remains stable, regardless of the parameters settings, enabling appropriate selection of the observer bandwidth. It is demonstrated that, based on the displacement signals generated by QPD, appropriately tuned NESOs can effectively estimate total disturbances, with target manoeuvres as dominant part. The simulation results show that, compared to controllers with LESOs, proposed scheme achieved better control performances in pointing to stationary targets and tracking of manoeuvring targets scenarios. The efficiency of the NESO-based ADRC in tracking errors compensation, is illustrated in both, the transient and the steady state.

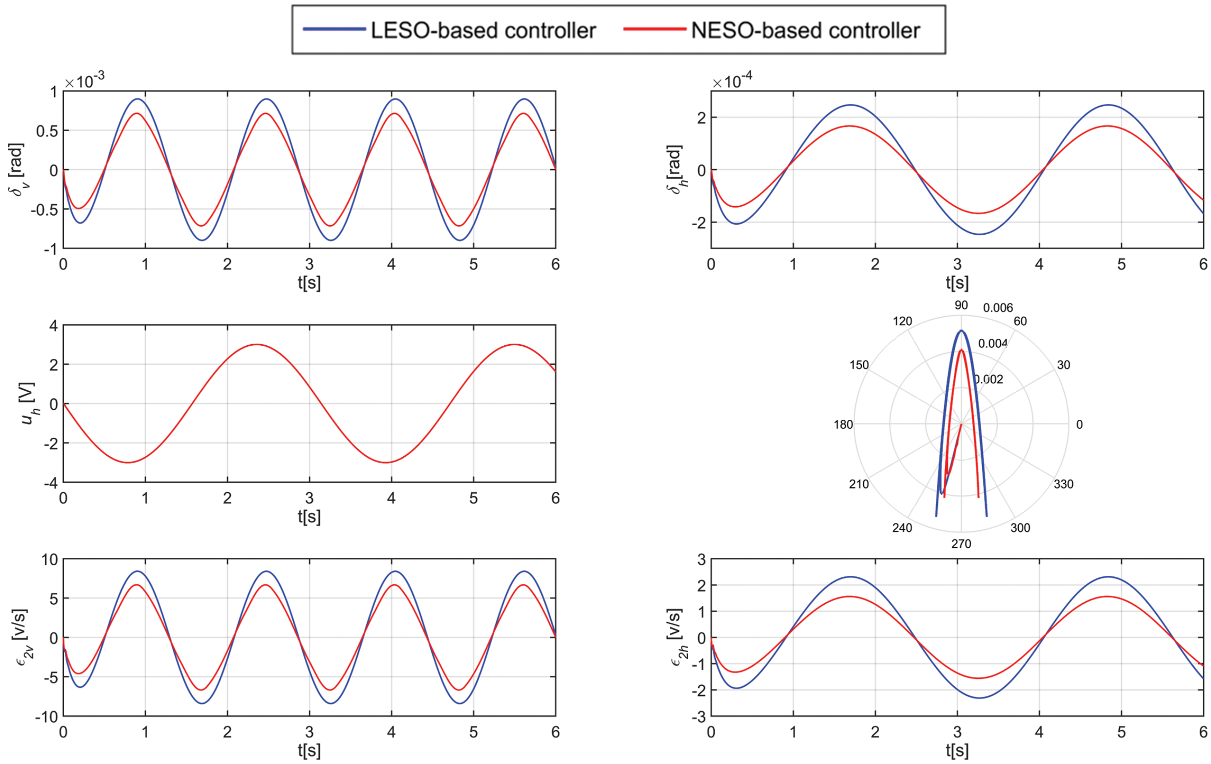

Figure 6. Simulation results for Scenario 3: tracking errors in vertical channel (top left), tracking errors in horizontal channel (top right), control signals in vertical control channel (middle left), spot centre trajectories (middle right), total disturbance error in vertical channel (bottom left), total disturbance error in horizontal channel (bottom right).

REFERENCES

1. Maini, N.; Sabharwal, A.; Sareen, K.; Singh, A. & Kumar, P. A user programmable electro-optic device for testing laser seekers. *Def. Sci. J.,* 2014, **64**(1), 88-92. doi: 10.14429/dsj.64.4857
2. Likun, Z. H. U.; Fangxiu, J. I. A.; Xiaodong, J. I. A. N. G. & Xinglong, L. I. Photoelectric detection technology of laser seeker signals. *J. Sys. Eng. Electronics*, 2019, **30**(6), 1064-1073. doi : 10.21629/JSEE.2019.06.02
3. Zhao, Y.; Han, D.; Wang, G. & Xiao, K. A Guidance Method Adapted to the Full Strap-Down Laser Homing System. In *2018 International Conference on Control, Automation and Information Sciences (ICCAIS)*. 2018, October, 275-278. IEEE. doi: 10.1109/ICCAIS.2018.8570495
4. Barbarić, Ž. P.; Lutovac, M. D. & Đokić, I. D. Analyses of probability density function of displacement signal for laser seeker systems. In 2011 10th International Conference on Telecommunication in Modern Satellite Cable and Broadcasting Services, 2011, October. **1**, 122-125. IEEE. doi: 10.1109/TELSKS.2011.6112019
5. Zhang, M.; Liu, H.; Zhang, H. & Miao, X. A hybrid control strategy for the optoelectronic stabilized platform of a seeker. *Opt.*, 2019, **181**, 1000-1012. doi: 10.1016/j.ijleo.2018.12.168
6. Barbarić, Ž. P.; Manojlović, S. M.; Bondžulić, B. P.; Andrić, M. S. & Mitrović, S. T. New relationship of displacement signal at quadrant photodiode: Control signal analysis and simulation of a laser tracker. *Opt.*, 2014, **125**(4), 1550-1557. doi: 10.1016/j.ijleo.2013.10.012
7. Abdo, M. M.; Vali, A. R.; Toloei, A. R. & Arvan, M. R. Improving two axes gimbal seeker performance using cascade control approach. *Proceedings of the Institution of Mechanical Engineers, Part G: J. Aerospace. Eng.*, 2015, **229**(1), 38-55. doi: 10.1177/0954410014525130
8. Abdo, M. M.; Vali, A. R.; Toloei, A. R. & Arvan, M. R. Stabilization loop of a two axes gimbal system using self-tuning PID type fuzzy controller. *ISA Transactions.*, 2014, **53**(2), 591-602. doi: 10.1016/j.isatra.2013.12.008
9. Lee, H. P. & Hwang, H. Y. Design of two-degree-of-freedom robust controllers for a seeker scan loop system. *Int. J. Control.*, 1997, **66**(4), 517-538. doi: 10.1080/002071797224577
10. Seong, K. J.; Kang, H. G.; Yeo, B. Y. & Lee, H. P. The stabilization loop design for a two-axis gimbal system using LQG/LTR controller. In *2006 SICE-ICASE International Joint Conference*, 755-759. IEEE. doi: 10.1109/SICE.2006.315268
11. Smith, B. J.; Schrenk, W. J.; Gass, W. B. & Shtessel, Y. B. Sliding mode control in a two-axis gimbal system. In *1999 IEEE aerospace conference. Proceedings (Cat. No. 99TH8403)*. **5**, 457-470. IEEE. doi: 10.1109/AERO.1999.790222
12. Hasturk, O.; Erkmen, A. M. & Erkmen, İ. Proxy-based sliding mode stabilization of a two-axis gimbaled

platform. World Congress on Engineering and Computer Science (WCECS 2011). 370-376. San-Francisco, Costa Rica

13. Bai, C. & Zhang, Z. A least mean square based active disturbance rejection control for an inertially stabilized platform. *Opt.*, 2018, **174**, 609-622. doi: 10.1016/j.ijleo.2018.08.099
14. Zhang, M.; Guan, Y. & Zhao, W. Adaptive super-twisting sliding mode control for stabilization platform of laser seeker based on extended state observer. *Opt.*, 2019 **199**(16), 163337. doi: 10.1016/j.ijleo.2019.163337
15. Manojlović, S. M.; Barbarić, Ž. P. & Mitrović, S. T. A novel active disturbance rejection based tracking design for laser system with quadrant photodetector. *Int. J. Control.*, 2015. **88**(6), 1246-1256. doi: 10.1080/00207179.2014.1002426
16. Stanković, M. R.; Madonski, R.; Shao, S. & Mikluc, D. On dealing with harmonic uncertainties in the class of active disturbance rejection controllers. *Int. J. Control.*, 2020, (just-accepted), 1-29. doi: 10.1080/00207179.2020.1736639
17. Madoński, R. & Herman, P. Survey on methods of increasing the efficiency of extended state disturbance observers. *ISA transactions.*, 2015, **56**, 18-27. doi: 10.1016/j.isatra.2014.11.008
18. Chen, W. H.; Yang, J.; Guo, L. & Li, S. Disturbance-Observer-Based Control and Related Methods—An Overview. *IEEE Transactions on Industrial Electronics.*, 2016, **63**(2), 1083. doi: 10.1109/TIE.2015.2478397
19. Łakomy, K. & Madonski, R. Cascade extended state observer for active disturbance rejection control applications under measurement noise. *ISA transactions*, 2020. doi: 10.1016/j.isatra.2020.09.007
20. Han, J. From PID to active disturbance rejection control. *IEEE transactions on Industrial Electronics.,* 2009, **56**(3), 900-906. doi: 10.1109/TIE.2008.2011621
21. Gao, Z. Scaling and bandwidth-parameterization based controller tuning. In *Proceedings of the 2003 American Control Conference., 2006.* **6**, 4989-4996. IEEE. doi: 10.1109/ACC.2003.1242516
22. Zhao, Z. L. & Guo, B. Z. On convergence of nonlinear active disturbance rejection control for SISO nonlinear systems. *J. of Dynamical and Control Systems.*, 2016, **22**(2), 385-412. doi: 10.1007/s10883-015-9304-5
23. Li, J.; Qi, X.; Xia, Y.; Pu, F. & Chang, K. Frequency domain stability analysis of nonlinear active disturbance rejection control system. *ISA transactions.*, 2015, **56**, 188-195. doi: 10.1016/j.isatra.2014.11.009
24. Li, J.; Xia, Y.; Qi, X. & Zhao, P. Robust absolute stability analysis for interval nonlinear active disturbance rejection based control system. *ISA transactions.*, 2017, **69**, 122-130. doi: 10.1016/j.isatra.2017.04.017
25. Wu, Z. H.; Zhou, H. C.; Guo, B. Z. & Deng, F. Review and new theoretical perspectives on active disturbance rejection control for uncertain finite-dimensional and infinite-dimensional systems. *Nonlinear Dynamics*, 2020, 1-25. doi: 10.1007/s11071-020-05845-7
26. Wu, D. & Chen, K. Frequency-domain analysis of nonlinear active disturbance rejection control via the describing function method. *IEEE Transactions on Industrial Electronics.*, 2012, **60**(9), 3906-3914. doi: 10.1109/TIE.2012.2203777
27. Chen, S.; Bai, W.; Hu, Y.; Huang, Y. & Gao, Z. On the conceptualization of total disturbance and its profound implications. *Science China Information Sciences.*, 2020, **63**(2), 129201. doi: 10.1007/s11432-018-9644-3
28. Li, J.; Xia, Y.; Qi, X. & Gao, Z. On the necessity, scheme, and basis of the linear–nonlinear switching in active disturbance rejection control. *IEEE Transactions on Industrial Electronics.*, 2016, **64**(2), 1425-1435. doi: 10.1109/TIE.2016.2611573
29. Stanković, M. R.; Manojlović, S. M.; Simić, S. M.; Mitrović, S. T. & Naumović, M. B. FPGA system-level based design of multi-axis ADRC controller. *Mechatronics.*, 2016, **40**, 146-155. doi: 10.1016/j.mechatronics.2016.10.005

ACKNOWLEDGMENT

The research is extensively supported by University of Defence in Belgrade, Military Academy, Belgrade, Serbia, under grant VA-TT/1/21-23.

CONTRIBUTORS

Mr Abdellah Ferdjali born in Bouira, Algeria, in 1991. He received the Engineering degree and the M.Sc degree in electrical engineering from Polytechnic Military School, Algiers, Algeria, in 2016. He is currently working toward the Ph.D. degree at University of Defence in Belgrade, Military Academy, Belgrade, Serbia. His research interests include guidance and robust control of multi-axis platforms.
His contribution consisted in modelling and designingthe active disturbance rejection control for the laser seeker system.

Mr Taki-Eddine Lechekhab was born in 1989, Khenchela, Algeria. He obtained the Master degree in advanced telecommunications from Abbas Laghror University, Khenchela, Algeria, in 2012. He is Ph.D. student in the Military Academy of Belgrade, University of defence. His current research interests include the embedded systems, Unmanned Aerial Vehicles, Quadrotors control laws and modelling, Active disturbance rejection control (ADRC).
His contribution consisted in modelling and designing the active disturbance rejection control for the laser seeker system.

Dr Stojadin Manojlović received his B.Sc. in Electrical Engineering from Military Academy of Belgrade, Serbia (2001), M.Sc. degree from Faculty of Electrical Engineering, University of Belgrade (2008) and Ph.D. degree from Military Academy of Belgrade, Serbia (2016). He is currently a Professor with

the Department of Military-electrical engineering, Military Academy of Belgrade, Serbia. His research interests include servo systems, guidance and control systems and digital design. He published over 20 papers in national and international conferences proceedings and journals.
His contribution consists in modelling the laser seeker system.

Dr Momir Stanković received his B.Sc. in Electrical Engineering from Military Academy of Belgrade, Serbia (2009) and Ph.D. degree from Faculty of Electronic Engineering, University of Niš, Serbia (2018). He is currently a Professor with the Department of Military-electrical engineering, Military Academy of Belgrade, Serbia. His research interests include design, optimisation and implementation of robust control systems. He published over 20 papers in national and international conferences proceedings and journals.
He is the principal investigator under which the research work reported in the paper was carried out.

Dr Rafal Madonski received his M.Sc. degree (2010) and Ph.D. degree (2016) from Poznan University of Technology, Poland. He is currently a Professor with the International Energy College, Jinan University, Guangzhou, China. His research interests focus on controlling uncertain systems, disturbance observers, as well as adaptive and robust control techniques. He published over 30 papers in international conferences proceedings and journals.
His contribution consists in verifying and supervising the architecture of proposed controllers.

Dr Dimitrije Bujakovic received the B.Sc. degree in electrical engineering from Military Technical Academy, Serbia in 2004, M.Sc. degree at the School of Electrical Engineering, University of Belgrade, Serbia in 2008 and Ph.D. degree from the School of Electrical Engineering, University of Belgrade, Serbia in 2016. He is an assistant professor at the Department of Military Electrical Engineering, Military Academy, University of Defence in Belgrade. His research interests include pattern recognition, control systems and methods for signals analysis and digital signal processing. He has published more than 40 papers in national and international conferences and journals.
His contribution consist on the discussion of the stability analysis using describing function method.